Available online at www.sciencedirect.com
SCIENCE DIRECT®
Surface Science 566–568 (2004) 13–23
SURFACE SCIENCE
www.elsevier.com/locate/susc

Mechanical properties and electrical conductance of different Al nanowires submitted to an homogeneous deformation: a first-principles simulation

Pavel Jelínek [a,b,*], Rubén Pérez [a], José Ortega [a], Fernando Flores [a]

[a] Departamento de Física Teórica de la Materia Condensada, Universidad Autónoma de Madrid, Modulo C-V, Campus Cantoblanco, Madrid E-28049, Spain

[b] Institute of Physics, Academy of Sciences of the Czech Republic, Cukrovarnická 10, 1862 53 Prague, Czech Republic

Available online 31 May 2004

Abstract

The evolution of the structure and conductance of different Al nanowires subject to a tensile stress has been studied by first-principles total-energy simulations combined with the non-equilibrium Keldysh Green's function approach for transport. Our calculations show the correlation between discontinuous changes in the total energy (associated to changes in the bonding structure of the nanowire) and abrupt modifications of the conductance as the nanowire develops a thinner neck, in agreement with the experiments. In spite of the quite different initial configurations and behaviour for some of the wires, in all the cases we obtain the same structure for the nanocontact during the last stages of the deformation process. The dimer geometry we have found for the nanocontact structure before the final breaking nicely reproduces the characteristic increase of the conductance in the last plateau and the presence of three conducting channels, one with a dominant contribution, giving the total conductance close to the quantum of conductance found in the experiments.

Keywords: Electrical transport (conductivity, resistivity, mobility, etc.); Surface stress; Metallic surfaces; Gold; Contact; Density functional calculations

1. Introduction

Nanocontacts between metallic leads have recently received a lot of attention [1]. The development in this field has mainly been stimulated by the invention of two techniques, the scanning tunneling microscope (STM) [2] and the mechanically controllable break junction (MCBJ) [3], that have allowed the gentle control of the distance between two metals. This way of operating allowed the experimental characterization of the atomic contacts and the observation of quantum effects in both their conductance and their forces [4]. One of the most interesting results for those nanocontacts has been the observation of several jumps in the conductance as a function of the nanocontact stretching; in particular, near the contact break point, when the neck of the wire is

* Corresponding author. Address: Departamento de Física Teórica de la Materia Condensada, Universidad Autónoma de Madrid, Modulo C-V, Campus Cantoblanco, Madrid E-28049, Spain. Tel.: +34-91-3978628; fax: +34-91-3974950.
E-mail address: pavel.jelinek@uam.es (P. Jelínek).

0039-6028/$ - see front matter © 2004 Elsevier B.V. All rights reserved.
doi:10.1016/j.susc.2004.05.014

defined by one or two atoms, the conductance jumps from a quantity that it is not far from the conductance quantum $\frac{2e^2}{h}$ to a zero value (tunneling region). It has been found that the value of this first jump in the conductance is quite close to this quantum for metals like Au and Al [5], while its value is a factor of two or three larger for transition metals, like Pd and Pt [6]. In a pioneering work, Scheer et al. [7] have shown, analyzing the superconducting properties of an atomic contact near its break point, how the electrical conductance of the system depends on a few channels that they relate theoretically to the orbitals associated with the atom (or atoms) of the wire neck.

The formation of necks and atomic contacts in stretched metallic nanowires has been analyzed theoretically with different approaches. Using molecular dynamics simulations with classical potentials, two groups showed in the early nineties [8,9] how the stretching of nanowire produces rearrangement of the atomic structure and the formation of a narrow neck. Other groups [10,11] have also used molecular dynamics simulations with effective-medium theory potentials for analyzing the same effect. While this represents a more accurate approach, it still lacks the accuracy and transferability provided by ab initio calculations based on the density functional theory (DFT) for describing the nanowire mechanical properties and the electronic structure needed for the calculation of the conductance. However, the large computational demand of this approach have restricted most of its applications to the analysis of model geometries where only a few atoms (3 or 4 typically) are allowed to relax [12–15]. Up to our knowledge, the most complete calculation of the mechanical properties and the electrical conductance of a metallic nanowire has been presented by Nakamura et al. [16] who analyzed, using a DFT-approach, a Na nanowire of 39 atoms. In this simulation the wire is elongated in steps of 0.2 or 0.4 Å until it reaches the break point. The conductance is determined using the Landauer–Buttiker formula, the corresponding transmission matrix being calculated using scattering techniques [17]. This calculation showed how the Na-nanowire stretching was accompanied by a rearrangement of the atomic configuration, that introduces jumps in the conductance and the forces of the system.

Our goal in this paper is to characterize the mechanical and conductance properties of stretched Al nanowires. Addressing this complex problem with a fully converged first-principles description would limit our calculations to a single wire geometry (as in the Na wire calculation discussed above), while different configurations are needed in order the explore the generality of the breaking process and the conductance behaviour to compare with the experimental evidence. One alternative is to stick to accurate plane wave DFT methods, carefully relaxing the conditions for convergence (basis set cutoff, k-point sampling etc.) [18]. A second alternative, which we follow in this paper, is to resort to local-orbital DFT methods, specially those derived with the aim of computational efficiency like the local-orbital minimal basis DFT code [19,20] we use, that allow first-principles studies of much more complex systems. This approach has an added value, as the transport properties of nanowires can be much more easily calculated from the resulting electronic hamiltonian (formally equivalent to a tight-binding or LCAO hamiltonian) using non-equilibrium Green's function techniques [21].

Closely related approaches [22–26], based on the combination of ab initio calculations on local-orbital basis and Keldysh–Green function methods, have been recently applied to characterize some ideal geometries (mainly, atomic chains) for Al and Au nanowires. At variance with these calculations, we have performed lengthy simulations of the whole breaking process of different Al nanowires in order to identify the structure of the nanocontact during the last stages of the deformation process. Our results show that all the different configurations lead to essentially the same dimer structure (not the ideal single-atom contact assumed by many authors) for the geometry of the nanocontact before the final breaking. In spite of the different initial values, the conductance reaches, at these last stages, a value close to the conductance quantum, with three channels (one dominant) contributing, in agreement with the experiment.

The rest of the paper is organized as follows: In Section 2, we present the different geometries for the nanowires we are going to consider and discuss

our way of analyzing it. After a brief comment on the performance of the local-orbital DFT technique we use for obtaining the nanowire structure along the stretching path, we discuss the Keldish–Green function method for the calculation of the electrical conductance and its connection with other approaches like the Fisher–Lee equation [27]. Our results for the evolution of the total energy, geometry and conductance for the different Al nanowires are presented in Section 3. We conclude in Section 4 with a discussion of the general properties of Al nanocontacts that can be deduced from our results and a comparison with the experimental evidence.

2. Model and method of calculation

Fig. 1 shows the schematic representation of the system we are interested in: a nanowire defined by several layers is located between two Al(1 1 1) surfaces. The initial configuration of the wire corresponds to the fcc stacking of a number n of (1 1 1) planes with typically three atoms per layer and it is oriented in the (1 1 1) direction as the surface layers simulating the two electrodes. The normal distance between the different (1 1 1) planes is taken equal to the Al bulk value. In this work, we focus on nanowires with $n = 4$, 5 and 8 layers.

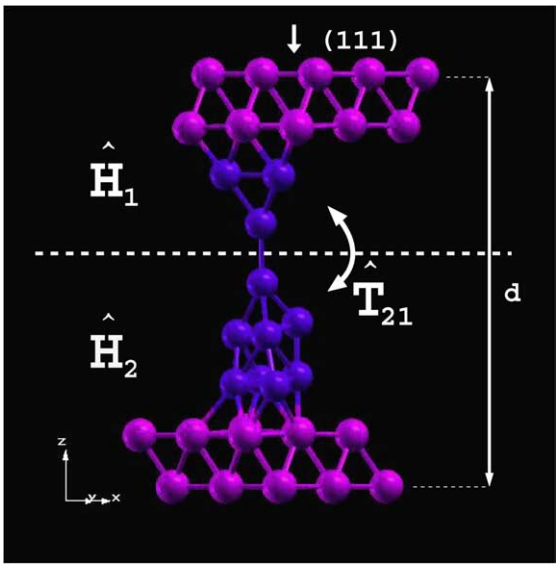

Fig. 1. Schematic geometry for a nanowire located between two Al(1 1 1) surfaces, acting as the electrodes. d is the distance between the fixed planes use to describe the stretching process.

We have used a supercell approach. In particular, we have considered a (3×3) periodicity in the direction parallel to the surface, that is large enough in most cases to decouple the different wires in neighbouring cells from each other. However, some of the calculations were affected by finite-size effects (see below) and have been repeated with a 4×4 periodicity. We have also imposed periodic boundary conditions in the direction perpendicular to the surface joining artificially the last two layers (top and bottom) of the system. This implies each electrode has effectively four (1 1 1) layers.

The ideal initial configuration for each of the nanowires is thus relaxed to the ground state keeping fixed the last two layers (top and bottom layers in Fig. 1) in order to simulate the bulk termination of the electrodes. These relaxed initial configurations for the $n = 4$, 5 and 8 nanowires correspond to the geometries labeled A in Figs. 2, 4 and 6. Notice that in the $n = 8$ case, the relaxed structure departs significantly from the initial ideal configuration, where a bend wire with a sort of stacking fault in the middle of the wire has replaced the initial fcc stacking.

The stretching of the system is simulated increasing the distance, d (see Fig. 1), between the two limiting layers by steps of 0.1 Å (0.2 Å in the calculations with the 4×4 periodicity). After each step, the system is allowed to relax towards its configuration of minimum energy. In this relaxation, only the atoms located in the last two layers remain fixed. This means that, for example, for the $n = 5$ ($n = 8$) nanowire with a 3×3 periodicity, 33 (42) atoms are allowed to relax. The most demanding cases correspond to 4×4 periodicity considered in some calculations, where 47 (58) atoms are relaxed for the $n = 5$ ($n = 8$) nanowire.

The total energy minimization is performed in this work using a fast local-orbital minimal basis pseudopotential DFT technique (Fireball96) [19]. This code offers a very favorable accuracy/efficiency balance if the atomic-like basis set is chosen carefully. In the case of Al, the valence electrons were described by s and p slightly excited

pseudoatomic orbitals [20]. For a cutoff radii $R_c = 6.4$ a.u. we obtained for fcc. Al a lattice parameter of $a = 3.97$ Å and a bulk modulus of $B = 74$ GPa (experiment: $a = 4.05$ Å, $B = 76$ GPa). The convergence criteria for the relaxation are changes in the total energy per atom less than 10^{-5} eV and forces on the free atoms less than 0.05 eV/Å. Our approach is complemented with PW-DFT-LDA calculations (using the CASTEP code [28]) performed at critical points of the nanowire deformation, as discussed below.

We have calculated the electrical conductance of the nanowire using a Keldish–Green function approach based on the first-principles tight-binding hamiltonian obtained from the Fireball96 code, at each point of the deformation path. In this formalism, we rewrite the hamiltonian describing the system as $\widehat{H}_1 + \widehat{H}_2 + \widehat{T}_{12}$, where the total system is splitted into two parts, 1 and 2, $\widehat{T}_{12}$ defining the coupling between both (see Fig. 1). Typically, we use the thinnest part of the nanowire to define the interface between those two subsystems. Then, the current across the interface is given by:

$$I = \frac{4\pi e^2}{\hbar} \times \int_{\infty}^{-\infty} \mathrm{Tr}\left[\widehat{T}_{12}\hat{\rho}_{22}(\omega)\widehat{D}^{\mathrm{r}}_{22}(\omega)\widehat{T}_{21}\hat{\rho}_{11}(\omega)\widehat{D}^{\mathrm{a}}_{11}(\omega)\right]\mathrm{d}\omega \times (f_1(\omega) - f_2(\omega)) \quad (1)$$

where $\hat{\rho}_{11}$ and $\hat{\rho}_{22}$ are the density of states matrices associated with the decoupled ($\widehat{T}_{12} = 0$) sides 1 and 2, respectively, while:

$$\widehat{D}^{\mathrm{r}}_{22} = \left[\hat{1} - \widehat{T}_{21}\hat{g}^{\mathrm{r}}_{11}(\omega)\widehat{T}_{12}\hat{g}^{\mathrm{r}}_{22}(\omega)\right]^{-1} \quad (2)$$

and

$$\widehat{D}^{\mathrm{r}}_{11} = \left[\hat{1} - \widehat{T}_{12}\hat{g}^{\mathrm{a}}_{22}(\omega)\widehat{T}_{21}\hat{g}^{\mathrm{a}}_{11}(\omega)\right]^{-1}; \quad (3)$$

$\hat{g}^{\mathrm{r}}_{ii}$ and $\hat{g}^{\mathrm{a}}_{ii}$ are the retarded and advanced Green function, respectively, of the decoupled sides, i. In Eq. (1) $f_i(\omega)$ is the Fermi distribution function associated with side i. Notice that defining the $\widehat{T}^{\mathrm{eff}}_{ij}$ matrices

$$\widehat{T}^{\mathrm{eff}}_{21} = \widehat{D}^{\mathrm{r}}_{22}\widehat{T}_{21} \quad (4)$$

and

$$\widehat{T}^{\mathrm{eff}}_{12} = \widehat{D}^{\mathrm{a}}_{11}\widehat{T}_{12}, \quad (5)$$

we can rewrite Eq. (1) as follows:

$$I = \int_{\infty}^{-\infty} \frac{4\pi e^2}{\hbar}\mathrm{Tr}\left[\widehat{T}^{\mathrm{eff}}_{12}\hat{\rho}_{22}(\omega)\widehat{T}^{\mathrm{eff}}_{21}\hat{\rho}_{11}(\omega)\right]. \quad (6)$$

This equation looks like the elementary lowest order tunneling current between sides 1 and 2, created by the effective tunneling coupling $\widehat{T}^{\mathrm{eff}}_{12}$. We stress that Eq. (6) includes all the multiple scattering processes at the interface: in this sense, Eq. (6) is exact and it can be applied to systems where $\widehat{T}_{12}$ is not small, as is the case discussed in this paper.

In this paper, we only analyze the nanowire differential conductance, $\frac{\mathrm{d}I}{\mathrm{d}V}$ that is given by:

$$G = \frac{\mathrm{d}I}{\mathrm{d}V} = \frac{4\pi e^2}{\hbar}\mathrm{Tr}\left[\widehat{T}_{12}\hat{\rho}_{22}(E_{\mathrm{F}})\widehat{D}^{\mathrm{r}}_{22}(E_{\mathrm{F}})\widehat{T}_{21}\hat{\rho}_{11}(E_{\mathrm{F}})\widehat{D}^{\mathrm{a}}_{11}(E_{\mathrm{F}})\right]. \quad (7)$$

For analyzing how many channels contribute to the conductance, we have rewritten Eq. (7) as follows:

$$G = \frac{\mathrm{d}I}{\mathrm{d}V} = \frac{2e^2}{h}\mathrm{Tr}\left[\hat{t}\hat{t}^{+}\right] \quad (8)$$

where $\hat{t} = 2\pi\hat{\rho}^{1/2}_{11}\widehat{T}^{\mathrm{eff}}_{12}\hat{\rho}^{1/2}_{22}$ and use of the cyclic property of the trace has been done. Eq. (8) makes contact between our approach and Landauer's formalism [29]. Here $\hat{t}$ defines the transfer matrix of the nanowire and we can analyze the contribution of the different channels to the differential conductance by diagonalizing it.

Before closing this section, it is convenient to make also contact between our approach for calculating the differential conductance (Eq. (7)), and the one used by other authors based on Fisher–Lee's equation that is defined by splitting the system into three parts, $\widehat{H}_1 + \widehat{H}_\alpha + \widehat{H}_2$, with the couplings $\widehat{T}_{1\alpha}$ and $\widehat{T}_{\alpha 2}$ (for example, in Fig. 1, $\widehat{H}_1$, can represent electrode 1, $\widehat{H}_2$ electrode 2, and $\widehat{H}_\alpha$ the nanowire). Using this representation the differential conductance between electrodes 1 and 2 is given by [27]:

$$\frac{\mathrm{d}I}{\mathrm{d}V} = \frac{4\pi e^2}{h}\mathrm{Tr}\left[\widehat{\Sigma}^{(1)}_{\alpha\alpha}\widehat{G}^{\mathrm{r}}_{\alpha\alpha}\widehat{\Sigma}^{(2)}_{\alpha\alpha}\widehat{G}^{\mathrm{a}}_{\alpha\alpha}\right] \quad (9)$$

where $G^{r}_{\alpha\alpha}$ and $G^{a}_{\alpha\alpha}$ are the retarded and the advanced Green's function of the coupled system (with $\widehat{T}_{1\alpha} \neq 0$ and $\widehat{T}_{\alpha 2} \neq 0$). In Eq. (9):

$$\Sigma^{1}_{\alpha\alpha} = \widehat{T}_{\alpha 1}\hat{\rho}_{11}\widehat{T}_{1\alpha} \tag{10}$$

and

$$\Sigma^{2}_{\alpha\alpha} = \widehat{T}_{\alpha 2}\hat{\rho}_{22}\widehat{T}_{2\alpha} \tag{11}$$

Introducing Eqs. (10) and (11) in (9), we can write Eq. (9) as follows:

$$\frac{dI}{dV} = \frac{4\pi e^2}{h}\mathrm{Tr}\left[\widehat{T}^{\mathrm{eff}}_{21}\hat{\rho}_{11}\widehat{T}^{\mathrm{eff}}_{12}\hat{\rho}_{22}\right] \tag{12}$$

where

$$\widehat{T}^{\mathrm{eff,r}}_{12} = \widehat{T}_{1\alpha}\widehat{G}^{r}_{\alpha\alpha}\widehat{T}_{\alpha 2} \tag{13}$$

and

$$\widehat{T}^{\mathrm{eff,a}}_{21} = \widehat{T}_{2\alpha}\widehat{G}^{a}_{\alpha\alpha}\widehat{T}_{\alpha 1} \tag{14}$$

Eq. (12) is, formally, similar to Eq. (7). The difference is the following: (a) in our approach $\widehat{T}^{\mathrm{eff}}_{12}$ is defined by the direct coupling between both sides, renormalized by the interface multiple scattering processes; (b) in Fisher–Lee's equation, $\widehat{T}_{12}$ appears as an effective coupling created by the electron propagation, $\widehat{G}_{\alpha\alpha}$, across the interface. However, in spite of these apparent differences, one can prove that both equations (8) and (12), are equivalent (see [30]).

3. Results

3.1. Total energy and structure for the different nanowires

Figs. 2 and 3 show the geometry and the total energy per unit cell of the nanowire as a function of the stretching displacement, Δd, for the $n = 4$ nanowire with a 3×3 periodicity. Figs. 4 and 5 (6 and 7) display similar results for the $n = 5$ ($n = 8$) nanowires.

Notice that all the total energy plots for the different nanowires (Figs. 3, 5 and 7) display discontinuities associated with the points where the nanowire suffers an important rearrangement in its

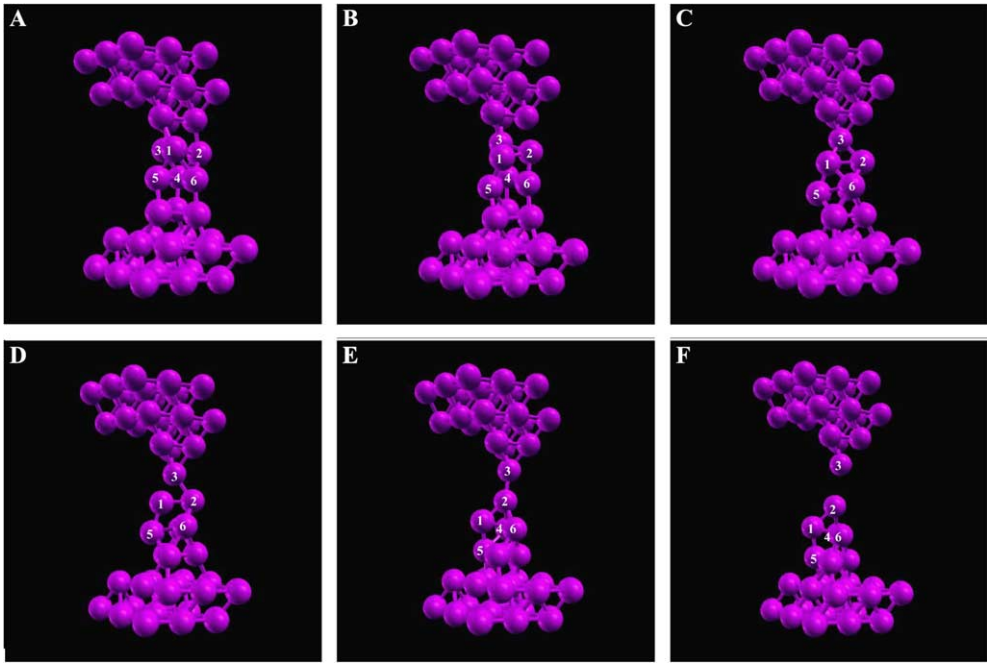

Fig. 2. Ball-and-Stick model of the structure of the nanowire geometry ($n = 4$) along the stretching process. Different cases corresponds to the points A, B, C, D, E and F of Fig. 3.

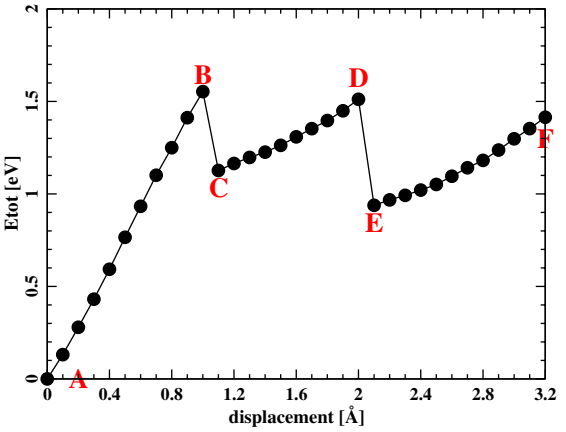

Fig. 3. Total energy (per unit cell) of the Al nanowire as a function of the stretching displacement, Δd, for $n = 4$.

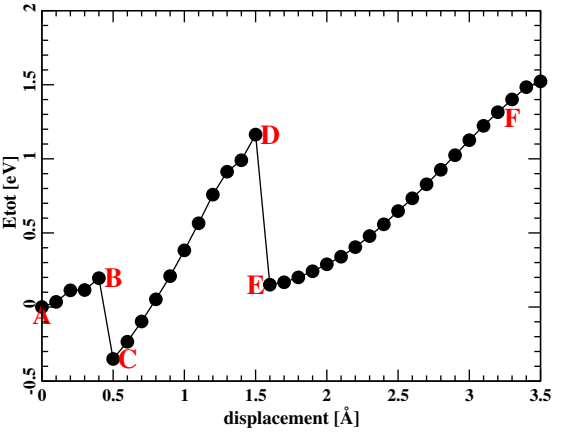

Fig. 5. Total energy (per unit cell) of the Al nanowire as a function of the stretching displacement, Δd, for $n = 5$.

bonding geometry. Figs. 2, 4 and 6 show snapshots of the nanowire geometry before and after the energy jumps (e.g. points labeled B, C and D, E in Fig. 5), together with the initial geometry (A) and the structure close to the final breaking point (F). Although the results for the $n = 4$ nanowire have been published elsewhere [31], they are also presented here for the sake of comparison.

It is worth comparing Figs. 3 and 5, for $n = 4$ and $n = 5$ respectively. Notice the similarity be-

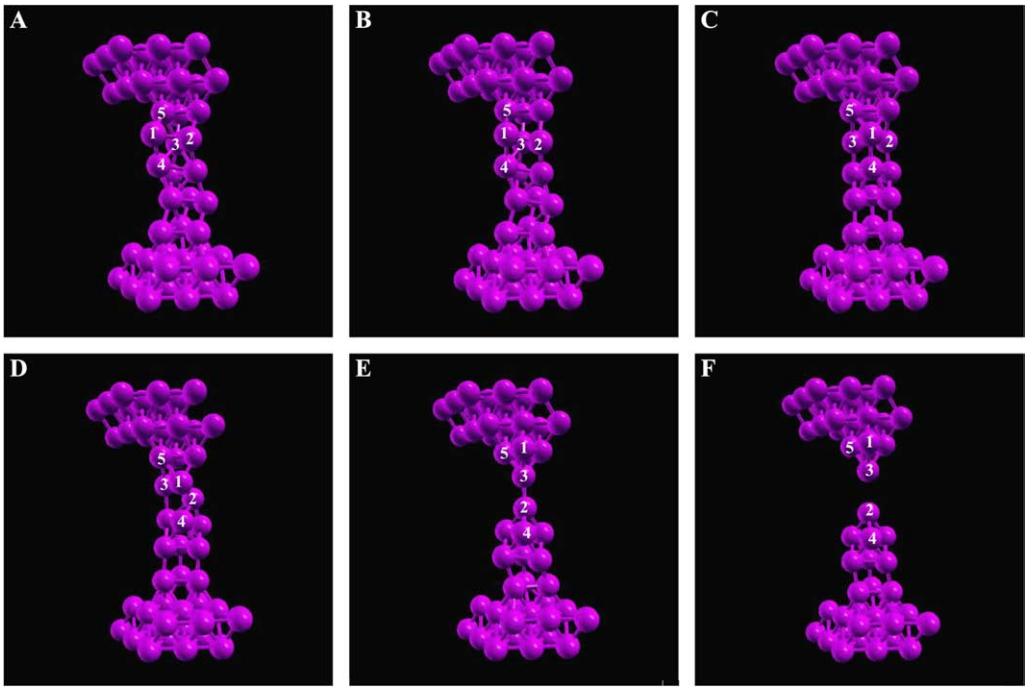

Fig. 4. Ball-and-Stick model of the structure of the nanowire geometry for $n = 5$. Different cases A, B, C, D, E and F, correspond to the points of Fig. 5.

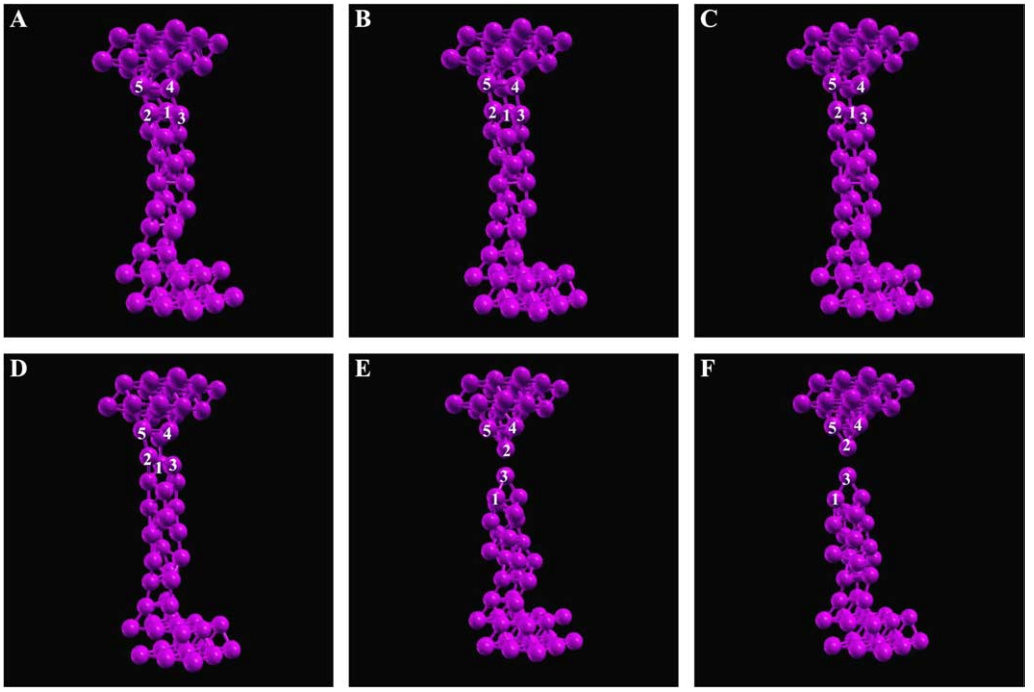

Fig. 6. Ball-and-Stick model of the structure of the Al nanowire $n = 8$ (see Fig. 7).

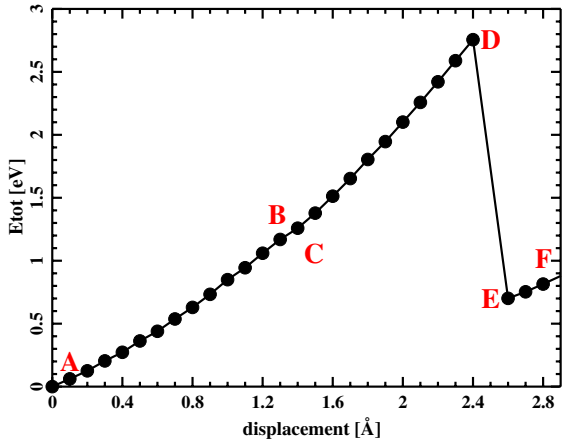

Fig. 7. Total energy (per unit cell) of the Al nanowire as a function of the stretching displacement, Δd, for $n = 8$.

tween both cases, although for $n = 5$ the stretching displacement for reaching the first and second jumps are a little smaller than for the case $n = 4$. In both cases, the main rearrangement of atoms occurs in the layer formed by atoms 1, 2 and 3. For $n = 5$ (see Fig. 4), there is a strong rearrangement of these atoms at the BC jump, while atom 2 moves out of this layer along the CD path. At the DE jump, atom 1 moves upwards and the narrowest neck is defined by the dimer 2–3, the nanowire reaching a geometry very similar to the one formed at the breaking point. Comparing these geometries with the ones corresponding to the $n = 4$ case (Fig. 2), we also find many similarities and a few differences. In particular, at the BC jump, atom 3 in $n = 4$ already takes an independent position between a layer of three atoms and the two atoms 1–2. The case D of this figure is, however, very similar to the case D of Fig. 4, with atom 3 linking a dimer and a layer of three atoms. After the point D, the $n = 4$ case, evolves pretty much like the $n = 5$ case; in particular, we also find a dimer 2–3 which defines the neck of this nanowire just before the break point.

We have checked the calculations for $n = 4$, obtained with the Fireball96 code, by recalculating geometries around the jumps (BC and DE) using the more accurate (but more computationally

demanding) CASTEP code. These calculations confirm the validity of the Fireball results; we have found, however, minor differences. For instance in CASTEP we find the system to present the first jump for $\Delta d = 0.9$ Å, namely, a step before the jump found by Fireball; the system evolves, however, across the first jump to the same geometry calculated with Fireball.

A closer inspection of the relaxed geometries for $n = 5$ reveals that some of our calculations may be affected by the finite size of our 3×3 simulation unit cell. This can be understood looking at the geometry E of Fig. 4, where atom 1 has finally moved up to the same layer of atom 5. At this configuration, atom 1 suffers a small, but not completely negligible, interaction with the atoms in the nearest neighbour nanowire that we introduce with the 3×3 periodicity. We have thus repeated the calculation for the stretching process, starting from the D geometry, using a 4×4 periodicity. Although we have found some slight changes in the total energy, they do not modify significantly the general comments presented above.

Next, we consider the nanowire of length $n = 8$. At variance, with the previous cases, there is only one significant jump in the total energy curve along the stretching deformation (see Fig. 7). The geometries displayed in Fig. 6 show that along the AB path, the bend in the initial relaxed configuration of the nanowire is gradually eliminated, up to point B where the wire is completely straight and the bonds between the different (1 1 1) layers start being stretched (path CD). The critical rearrangement of atoms takes place at the DE jump (see Fig. 7) and involves the atoms around the plane 1–2–3. Related displacements are already taking place along the path ABCD, where atom 1 moves down and atom 2 moves up. At point D, the system jumps to a different bonding configuration, such that at point E we find the atom 1 around the plane of atoms located initially underneath, and the atom 3 has moved up forming the dimer 2–3 which now defines the nanowire neck. Along the EF path, the system is deformed, increasing basically the dimer length, 2–3, until reaching the break point.

Comparing this case, $n = 8$, with the shorter nanowires, $n = 4$ and $n = 5$, we find some striking similarities: (i) the most interesting one is the geometry appearing just before the breaking point. For all the cases, $n = 4$, 5 and 8, we find a dimer (2–3 in all the nanowires) at the neck. This dimer is closely related to the conductance properties that we discuss below. (ii) The second point to remark is the position of the breaking layer for the different nanowires. In all cases we find that breaking layer (the 1–2–3 layer) is located next to the layer of the lead–nanowire contact: one can speculate that this is an effect associated with local stress induced by the junction between the lead and the nanowire. (iii) We also mention that the evolution of the nanowire geometry along the stretching deformation is similar in all the cases, although for $n = 8$, the two jumps observed for $n = 4$ and 5 appear combined in a single jump whereby the final dimer geometry (case E of Fig. 6) develops.

3.2. Conductance along the stretching path

Let us now discuss the differential conductance for the three cases studied, $n = 4$, 5 and 8, as a function of the stretching displacement. Figs. 8–10 display our results: in all the cases, we also show the partial contribution of the different channels to the total conductance.

Fig. 8 corresponds to the case $n = 4$: the conductance shows two jumps in agreement with the

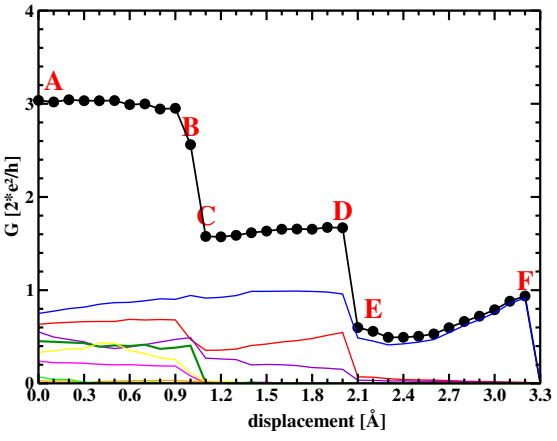

Fig. 8. Total differential conductance (in units of the conductance quantum) and channel contributions along the stretching path, for $n = 4$.

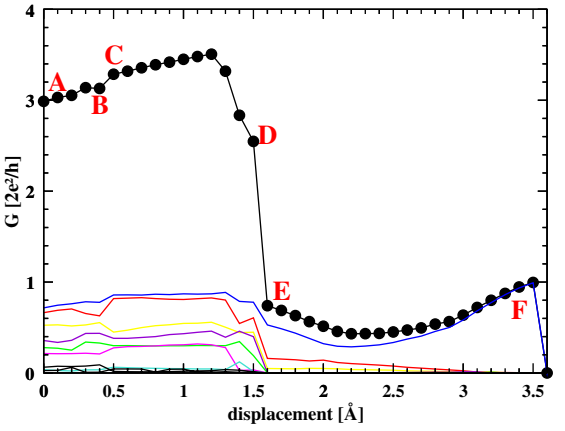

Fig. 9. Total differential conductance and channel contribution along the stretching path (as Fig. 8), for $n = 5$.

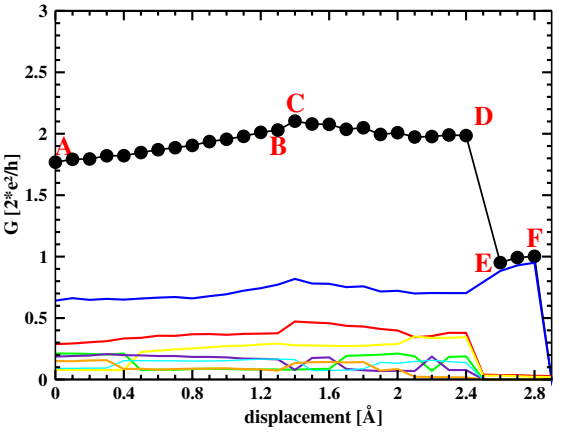

Fig. 10. Total differential conductance (in units of the conductance quantum) and channel contribution along the stretching path (as Fig. 8), for $n = 8$.

jumps we have found for the energy and the geometry. The evolution of the differential conductance, G, is the following: initially $G \approx 3(\frac{2e^2}{h})$ and it remains almost constant until close to B; the jump B–C, leaves G around $1.6(\frac{2e^2}{h})$; in the jump DE, the conductance decreases to $\approx 0.6(\frac{2e^2}{h})$ and, along the path EF, it increases to $\approx 0.98(\frac{2e^2}{h})$, almost the conductance quantum.

For $n = 5$ (see Fig. 9) the initial value of the conductance is again close to $3(\frac{2e^2}{h})$. Then, the conductance slightly increases along the path AB. The jump BC in the total energy gives a very modest change in the conductance (although it is clearly reflected in the contribution of the different eigenchannels). From C the conductance increases up to a maximum value of $3.5(\frac{2e^2}{h})$ at the point in the CD path where a change in the curvature of the total energy curve can be identified (see Fig. 5), and then decreases to $2.5(\frac{2e^2}{h})$ at D. In the second jump, DE, a number of channels close and G decreases to $\approx 0.7(\frac{2e^2}{h})$. In the final stage of the stretching displacement, G increases slowly until the break point, F, where the nanowire conductance takes a value close to $(\frac{2e^2}{h})$.

The conductance behaves in a similar way for the $n = 8$ case (see Fig. 10). The initial value, close to $1.8(\frac{2e^2}{h})$, differs from the results for the other nanowires and it is related more to the bend configuration of the nanowire. Along the AB path, the conductance increases up to a value close to $2.1(\frac{2e^2}{h})$ at B, where it shows a small jump going to C that we can associate to a small wiggle appearing in the curve of the nanowire energy (see Fig. 7). This is reminiscent of the small BC jump we find for $n = 5$. After that jump the conductance decreases slowly to a value around $2(\frac{2e^2}{h})$ at D. After the DE jump, the conductance increases until reaching a value close to the conductance quantum, $\approx 1.0(\frac{2e^2}{h})$.

Comparing these three cases we find common features in the evolution of the differential conductance as a function of the stretching deformation, although the initial values of the nanowire conductance is $3.02(\frac{2e^2}{h})$ ($n = 4$), $2.98(\frac{2e^2}{h})$ ($n = 5$) and 1.77 ($n = 8$) differ due to the different initial configurations. In all cases, there appear two jumps between this initial point and the final stage of the nanowire. Finally at the breaking point, G takes values close to $(\frac{2e^2}{h})$ but slightly different in all the cases: $0.98(\frac{2e^2}{h})$ ($n = 4$), $0.99(\frac{2e^2}{h})$ ($n = 5$) and $1.01(\frac{2e^2}{h})$ ($n = 8$). These are fluctuations that have been observed experimentally. We should also comment that in the last stage of the evolution of G we find, in all the cases, an increase of the differential conductance with the stretching displacement, a result that is also in agreement with the experimental evidence.

Figs. 8–10 also show how different channels contribute to the total differential conductance in the nanowire. All the cases show a common

feature: near the break point, we find that only three channels yield appreciable contribution to the total current, although there appears a predominant mode, very much in agreement with the results published by Scheer et al. [7]. Initially, $\Delta d = 0$, the systems are slightly different; for $n = 4$ and $n = 5$ we have eight markedly contributing channels, for $n = 8$ we only find seven channels. However, we should say that the cases $n = 5$ and $n = 8$ are very similar along the stretching path since it is only in the last jump when the six or seven channels are reduced to the three channels of the final stage.

4. Discussion and conclusions

The aim of this paper has been to analyze the mechanical and electrical conductance properties of different Al nanowires located between two Al(1 1 1) surfaces. Using an efficient first-principles local-orbital DFT method we have shown first, how to look for the geometry of the stretched nanowire as a function of the wire elongation up to the breaking point and, second, how to analyze its electrical conductance. This property has been studied using Keldish–Green functions techniques based on the analysis of the LCAO-hamiltonian afforded by our DFT calculations.

Our results show that, in spite of the quite different initial behaviour between some of the nanowires considered, in all the cases we obtain the same structure for the nanocontact during the last stages of the deformation process. The dimer geometry we have found for the nanocontact structure before the final breaking nicely reproduces the presence of three conducting channels, one with a dominant contribution, giving the total conductance close to the quantum of conductance found in the experiments. However, it differs significantly from all the assumed geometries discussed in the literature, and, in particular, from the ideal single atom contact. The fact that we also reproduce the characteristic increase of the conductance in the last plateau (not found in any previous ab initio study) indicates that the geometry found in our calculations is a fair representation of the deformation appearing near the breaking of the nanocontact.

Our DFT calculations show that the nanowire suffers important rearrangements of its bonding configuration as it deforms along the stretching path and how these changes affect its mechanical and conductance properties. These changes are reflected as discontinuous jumps in the total energy curve as the system moves between two stable configurations when the energy barrier between them goes to zero due to the stretching. These plastic deformations appear probably not only in the jumps mentioned above but also at some other points that are not so easily identified in the total energy curve. A case like this was found for $n = 8$, where the structural change in BC produces a discontinuity in the conductance rather than the slope change that we can see in the energy curve. This behaviour reflects the complicated energy landscape associated with the nanowire deformation, with many competing structures that are very close in energy.

We have analyzed this point in more detail by considering the reverse deformation of the nanowire with $n = 4$, starting near the break point, F, found in Fig. 2. Fig. 11 shows the energy of this case compared with the one calculated in Fig. 8: the important point to notice is that the energy of the compressive deformation is all the time below the one calculated for the stretching deformation,

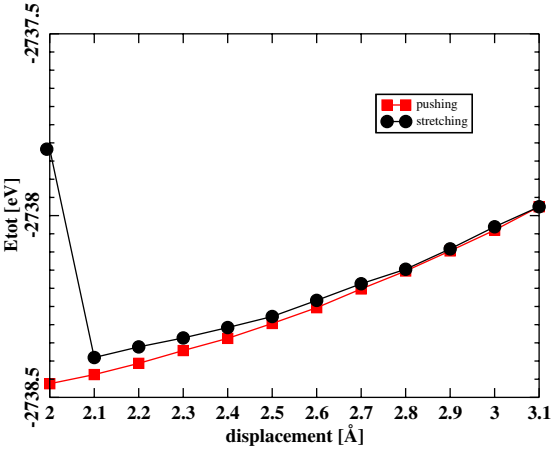

Fig. 11. Total energy (per unit cell) of the Al nanowire as function of stretching and compressive deformation.

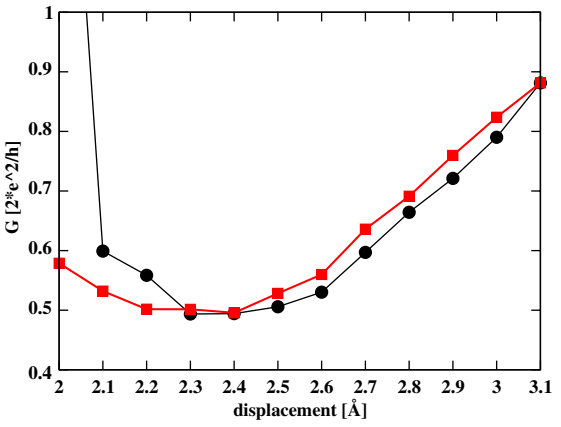

Fig. 12. Total differential conductance along the reverse processes of the Al nanowire deformation.

indicating that along the stretching path, EF, the system has suffered some small irreversible changes in the bonding configuration that prevent the system to recover the E-geometry. This is a real effect that reflects also in the calculated electrical conductance for the compressive deformation (see Fig. 12): we have found that, in this case, its value is a little larger than the one obtained along the stretching deformation: in spite of this increase, the differential conductance still presents qualitatively the same behaviour as a function of Δd.

Acknowledgements

P.J. gratefully acknowledges financial support by the European project no. HPRN-CT-2000-00154. This work has been supported by the DGI-MCyT (Spain) under contract MAT2001-0665.

References

[1] N. Agräit, A. Levy-Yeyati, J. van Ruitenbeek, Phys. Rep. 377 (2003) 81.
[2] G. Rubio-Bollinger, N. Agräit, S. Vieira, Phys. Rev. Lett. 76 (1996) 2302.
[3] E. Scheer, N. Joyez, D. Esteve, C. Urbina, M.H. Devoret, Phys. Rev. Lett. 78 (1997) 3535.
[4] G. Rubio-Bollinger et al., Phys. Rev. Lett. 87 (2001) 026101.
[5] J.C. Cuevas, A. Levy Yeyati, A. Martin-Rodero, G. Rubio Bollinger, C. Untiedt, N. Agraït, Phys. Rev. Lett. 81 (1998) 2990.
[6] C. Sirvent et al., Phys. Rev. B 53 (1996) 16036.
[7] E. Scheer, N. Agrait, J.C. Cuevas, A. Levy Yeyati, B. Ludoph, A. Martín-Rodero, G.R. Bollinger, J.M. van Ruitenbeek, C. Urbina, Nature 394 (1998) 154.
[8] U. Landman, W.D. Ludetke, B.E. Salisbury, R.L. Whetten, Phys. Rev. Lett. 77 (1996) 1362.
[9] T.N. Todorov, A.P. Sutton, Phys. Rev. Lett. 70 (1993) 2138.
[10] A.M. Bradkovsky, A.P. Sutton, T.N. Todorov, Phys. Rev. B 52 (1995) 5036.
[11] M.R. Sörensen, M. Brandbyge, K.W. Jacobsen, Phys. Rev. B 57 (1998) 3283.
[12] N.D. Lang, Phys. Rev. B 52 (1995) 5335.
[13] C.C. Wan, J.-L. Mozos, G. Taraschi, J. Wang, H. Guo, Appl. Phys. Lett. 71 (1997) 419.
[14] N. Kobayashi, M. Brandbyge, M. Tsukada, Phys. Rev. B 62 (2000) 8430.
[15] N. Kobayashi, M. Brandbyge, M. Tsukada, Surf. Sci. 433–435 (1999) 854.
[16] A. Nakamura, M. Brandbyge, L.B. Hansen, K.W. Jacobsen, Phys. Rev. Lett. 82 (1999) 1538.
[17] K. Hirose, M. Tsukada, Phys. Rev. B 51 (1995) 5278.
[18] D. Krüger, H. Fuchs, R. Rousseau, D. Marx, M. Parrinello, Phys. Rev. Lett. 89 (2002) 186402.
[19] A. Demkov, J. Ortega, O.F. Sankey, M.P. Grumbach, Phys. Rev. B 52 (1995) 1618.
[20] O.F Sankey, D.J. Nikelewski, Phys. Rev. B 40 (1989) 3979.
[21] N. Mingo, L. Jurczyszyn, F.J. Garcia-Vidal, R. Saiz-Pardo, P.L. de Andres, F. Flores, S.Y. Wu, W. More, Phys. Rev. B 54 (1996) 2225.
[22] G. Taraschi, J.-L. Mozos, C.C. Wan, H. Guo, J. Wang, Phys. Rev. B 58 (1998) 13138.
[23] H. Mehrez, A. Wlasenko, B. Larade, J. Taylor, P. Grutter, H. Guo, Phys. Rev. B 65 (2002) 195419.
[24] M. Brandbyge, J.-L. Mozos, P. Ordejon, J. Taylor, K. Stokbro, Phys. Rev. B 65 (2002) 165401.
[25] J.J. Palacios, A.J. Perez-Jimenez, E. Louis, E. SanFabian, J.A. Verges, Phys. Rev. B 66 (2002) 35322.
[26] J. Heurich, J.C. Cuevas, W. Wenzel, G. Schön, Phys. Rev. Lett. 88 (2002) 256803.
[27] D.S. Fisher, P.A. Lee, Phys. Rev. B 23 (1983) 6851.
[28] CASTEP 4.2 Academic version, licensed under the UKCP-MSI Agreement, 1999 M.C. Payne et al., Rev. Mod. Phys. 64 (1992) 1045.
[29] R. Landauer, Philos. Mag. 21 (1970) 863.
[30] F.J. García-Vidal, F. Flores, S.G. Davison, Prog. Surf. Sci. 74 (2003) 177.
[31] P. Jelinek, R. Perez, J. Ortega, F. Flores, Phys. Rev. B 68 (2003) 085403.